Sunlight-Coordinated High-Performance Moisture Power in Natural Conditions

Jiaxin Bai, Yaxin Huang, Haiyan Wang, Tianlei Guang, Qihua Liao, Huhu Cheng, Shanhao Deng, Qikai Li, Zhigang Shuai,* and Liangti Qu*

It is a challenge to spontaneously harvest multiple clean sources from the environment for upgraded energy-converting systems. The ubiquitous moisture and sunlight in nature are attractive for sustainable power generation especially. A high-performance light-coordinated "moist-electric generator" (LMEG) based on the rational combination of a polyelectrolyte and a phytochrome is herein developed. By spontaneous adsorption of gaseous water molecules and simultaneous exposure to sunlight, a piece of 1 cm^2 composite film offers an open-circuit voltage of 0.92 V and a considerable short-circuit current density of up to 1.55 mA cm^{-2}. This record-high current density is about two orders of magnitude improvement over that of most conventional moisture-enabled systems, which is caused by moisture-induced charge separation accompanied with photoexcited carrier migration, as confirmed by a dynamic Monte Carlo device simulation. Flexible devices with customizable size are available for large-scale integration to effectively work under a wide range of relative humidity (about 20–100%), temperature (10–80 °C), and light intensity (30–200 mW cm^{-2}). The wearable and portable LMEGs provide ample power supply in natural conditions for indoor and outdoor electricity-consuming systems. This work opens a novel avenue to develop sustainable power generation through collecting multiple types of natural energy by a single hybrid harvester.

1. Introduction

Environmental energy conversion technologies are promising for retarding the depletion of fossil fuels and the severe energy crisis.[1] The well-known examples include solar cells,[2] wind turbines,[3] thermoelectric generators,[4] and piezoelectric/triboelectric nanogenerators.[5] Significant advances have been accordingly made to effectively collect renewable energy from the environment, although they rely on solar radiation, wind power, temperature difference, and mechanical force, respectively.

In recent years, atmospheric moisture enabled electric generation (MEG) has attracted increasing attention owing to ubiquitous gaseous water molecules in the air. This kind of water-enabled power generators achieves considerable electricity output utilizing abundant water moisture in nature with simple device setup and by-produced pollutant excluded.[6] For MEG, single hygroscopic material with proper ionizable functional groups could release the free charged ions upon spontaneously adsorbing water molecules. Subsequently, the gradient of ion concentration formed by a chemical-gradient structure[7] or asymmetric moisturizing regulation[8] drives the charged ions to diffuse directionally, which leads to charge separation and thus gives rise to an electric potential between two sides of the applied MEG architecture. Such adsorption-based electricity generation extended into other systems by follow-up studies.[9] The induced voltage has reached a considerable level through chemical modification and microstructure control on hydrophilic materials.[7c,10] However, the current density of device unit is still unsatisfactory (≈10 μA cm^{-2}) and incapable to meet the demand of commercial electronics (>1 mA cm^{-2}), which could be ascribed to the limited carrier capacity and unsophisticated configuration in MEG.

In nature, assimilating various energy from environment collaboratively is apparently present in numerous natural ecosystems. For example, water-imbibed cells and chlorophyll in plants absorb water and sunlight synergistically to maintain normal life activities.[11] Inspired by this energy production process, we develop the first example of a highly efficient light-coordinated "moist-electric generator" (LMEG) based on the rational combination of hydrophilic polyelectrolyte with photosensitive phytochrome, as well as the mediation of electrodes/materials interfaces (**Figure 1**a). The hybrid LMEGs can harvest multiple sources of moisture and sunlight synchronously from surrounding environment without artificial intervention.

J. Bai, Y. Huang, T. Guang, Q. Liao, H. Cheng, L. Qu
State Key Laboratory of Tribology
Department of Mechanical Engineering
Tsinghua University
Beijing 100084, China
E-mail: lqu@mail.tsinghua.edu.cn
H. Wang, H. Cheng, S. Deng, Q. Li, Z. Shuai, L. Qu
Key Laboratory of Organic Optoelectronics and Molecular Engineering,
Ministry of Education
Department of Chemistry
Tsinghua University
Beijing 100084, China
E-mail: zgshuai@tsinghua.edu.cn

The ORCID identification number(s) for the author(s) of this article can be found under https://doi.org/10.1002/adma.202103897.
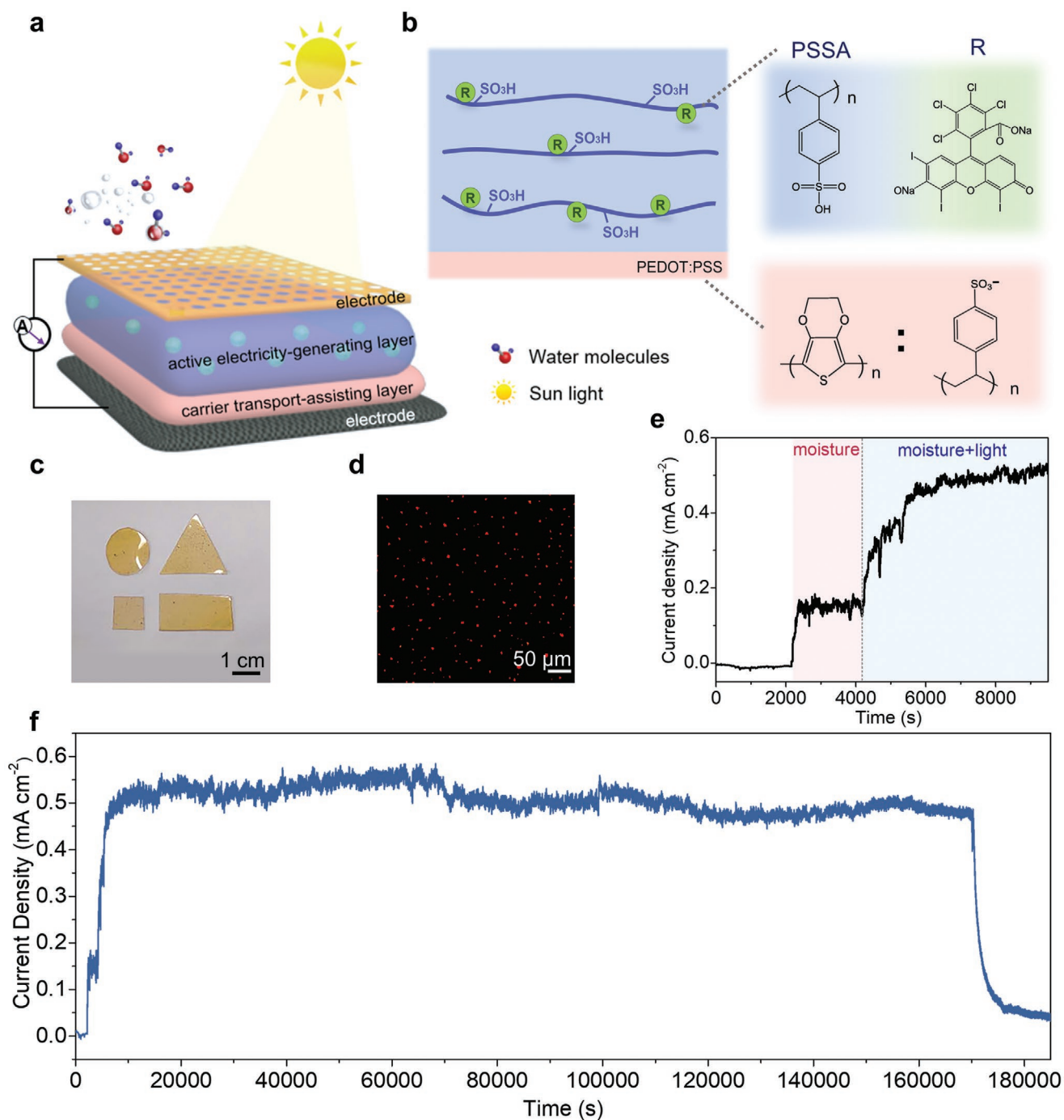
Figure 1. Prototype of the LMEG and corresponding electric output. a) A well-designed LMEG can harvest moisture and sunlight synchronously to enhance power output. The transport-assisting layer blocks electrons moving to the bottom electrode for further regulating flow direction of carriers, largely promoting the electric generation. b) PSSA/R film composed of PSSA matrix and R clusters. A PEDOT:PSS layer was spin-coated on the bottom electrode in close contact with the PSSA/R film. c) Photograph of the tailored PSSA/R films. d) CLSM image of PSSA/R film. The bright red spots correspond to R clusters. e) I_{sc} output under 50% RH further enhances after one sun illumination. f) I_{sc} output of an LMEG lasting for about 40 h under constant 50% RH, 100 mW cm^{-2}.

They produce a stable open-circuit-voltage of up to 0.92 V and a record-high short-circuit current density of 1.55 mA cm^{-2}. Benefiting from large-area manufacture and tailorable property, the scalable integration of flexible LMEGs supplies sufficient power to sailing a small speedboat on water and provides a versatile platform for the construction of portable and wearable power supply systems for indoor and outdoor electricity-consuming devices in ambient environment. This work provides insight to harvest multiple potential energy in the natural atmosphere for efficient electricity generation.

**ADVANCED
SCIENCE NEWS**
www.advancedsciencenews.com

**ADVANCED
MATERIALS**
www.advmat.de

2. Results and Discussions

2.1. Characterization and Electrical Performance of an LMEG

The active electricity-generating layer is constructed by the combination of a hygroscopic matrix of poly(4-styrensulfonic acid) (PSSA) with a photosensitive phytochrome (rose bengal (R)) into a free-standing hybrid film (PSSA/R) after the casting process (Figure 1b; Figure S1, Supporting Information). The tailorable semitransparent film can be customized to different geometries and sizes on demand (Figure 1c). Confocal laser scanning microscopy (CLSM) imaging clearly shows that R clusters with diameters ranging from 2.8 to 8.3 µm are uniformly dispersed in PSSA matrix (Figure 1d).

For electrical measurements, this flat PSSA/R film with thickness of about 0.56 mm (Figure S2, Supporting Information) was sandwiched between two electrodes for an LMEG unit. The upper electrode was manufactured with holes to ensure the effective access of moisture and sunlight to PSSA/R film. The bottom electrode was sealed and spin-coated in advance with poly(3,4-ethylenedioxythiophene):poly(styrene sulfonate) (PEDOT:PSS) to tailor carrier transport (Figure S3, Supporting Information).[12] When moisture approaches to the LMEG, an obvious short-circuit current density (I_{sc}) of 0.12–0.16 mA cm^{-2} is detected (RH = 50%, 25 °C). Intriguingly, the I_{sc} amplitude further increases to 0.49–0.57 mA cm^{-2} upon one sun illumination (Figure 1e; Figure S4, Supporting Information). The current retention of LMEG is 88% for more than 40 h, reflecting its outstanding stability (Figure 1f; Figures S5 and S6, Supporting Information). When an LMEG is exposed to illumination, the moisture-induced open-circuit voltage (V_{oc}) of 0.83 V increases to 0.92 V (Figure S7, Supporting Information). The V_{oc} curve shows a similar pattern to that of I_{sc}. The balanced performance of high current and voltage will facilitate feasible power output, displaying a maximum power density of up to 88 µW cm^{-2} (Figure S8, Supporting Information). These performances are repeatable for a long-term test (Figure S9, Supporting Information). In addition, LMEG viably exerts remarkable performance and stability under bending or pressing, implying its endurance for mechanical deformations (Figures S10 and S11, Supporting Information).

The appropriate thickness and weight ratio of R to PSSA in composite films are important to the electric performance of LMEG. PSSA/R film with a thickness of 0.56 mm can deliver an optimum I_{sc} (Figure S12, Supporting Information). I_{sc} increases along with the content of R and reaches a maximum value of 0.57 mA cm^{-2} in PSSA/R sample containing 0.2 wt% R (**Figure 2**a), while further increasing the ratio of R to PSSA results in a decline on power generation. This decline is relative to the weakened light absorption. The efficiency of light absorption is determined by

$$\alpha = 10^{-16} N_c \tag{1}$$

where N_c is the concentration of absorption centers for light harvesting and exciton generation, α is the absorption coefficient.[14] Attributed to appropriate content of R and the tight interaction of composites (Figures S13 and S14,

Supporting Information), R clusters can uniformly disperse on PSSA chains for efficient light absorption (Figure S15a, Supporting Information). However, the overmuch ratio of R to PSSA causes its severe agglomeration (Figure S15b–d, Supporting Information) resulting in decreased N_c and reduces efficiency of light absorption adverse to electric output.[15] To confirm the specific influence of natural sources, moisture and solar illumination are applied to an LMEG separately (Figure 2b). The I_{sc} reaches a maximum value of ≈0.16 mA cm^{-2} upon moisture incoming solely (RH = 50%), which is comparable to the reported MEGs.[8c] When light (100 mW cm^{-2}) illuminates the sample in the absence of moisture, the instantaneous photocurrent occurs, followed by rapid decline near to zero, which suggests the recombination of photogenerated carriers.[16] Remarkably, the electric output of LMEG under moisture and light simultaneously is much higher and more stable than the performance induced by single source. As shown in Figure 2c, I_{sc} increases from 0.1 to 0.48 mA cm^{-2} when light is turned on, with the I_{light}/I_{dark} ratio of 4.4. The above results indicate that light illumination and moisture adsorption jointly boosts power output of LMEG.

Light intensity has the influence of positive correlation on the performance of I_{sc}. As shown in Figure 2d, Figures S16–S19 and Tables S1–S3, Supporting Information, I_{sc} ascends with increasing incident intensity, which implies that more photo-excited charge carriers are available under higher light intensity.[17] Impressively, a considerable value of I_{sc} reaches about 0.84 mA cm^{-2} at 200 mW cm^{-2}. Even at the low light intensity of 50 mW cm^{-2}, LMEG can proactively deliver an I_{sc} of 0.32 mA cm^{-2} (50% RH). On the other hand, the surrounding RH has also significant effect on the performance of LMEG. Under high RH, I_{sc} of LMEG is visibly enhanced owing to the beneficial water adsorption (Figure 2d; Figure S19 and Table S1, Supporting Information). The dependence of I_{sc} on RH (50–100%) demonstrates that power generation is directly related to the hydration level of PSSA/R film exposed to humid environment,[13d] which will induce efficiently directional migration of H$^+$ ions.[6c] Furthermore, it is worth noting that LMEG is applicable in a wide range of ambient temperature from 25 to 80 °C and realizes a maximum value of 1.21 mA cm^{-2} at 60 °C (Figure 2e; Figure S19, Supporting Information), which could be attributed to the balanced adsorption of water molecules and transport of ions at an appropriate temperature (Figures S20 and S21, Supporting Information).[8b,d,18] The electric generation ability over a broadly workable range of light intensity, RH, and temperature makes LMEG possible to function in most regions on the earth. It will alleviate the regional constraints of previous MEGs that mainly work under artificial conditions in laboratory. After systematical adjustments of surrounding conditions, LMEGs exhibit the optimal I_{sc} of 1.55 mA cm^{-2} under 200 mW cm^{-2} light intensity, 100% RH and 60 °C. As illustrated in Figure 2f, Figures S22 and S23, Supporting Information, the output performance of LMEG provides both high voltage of 0.92 V and current density of 0.87 mA cm^{-2}, which is two orders of magnitude higher than that of most devices reported previously based on a single source of moisture under the same conditions.[7,8,10,13]
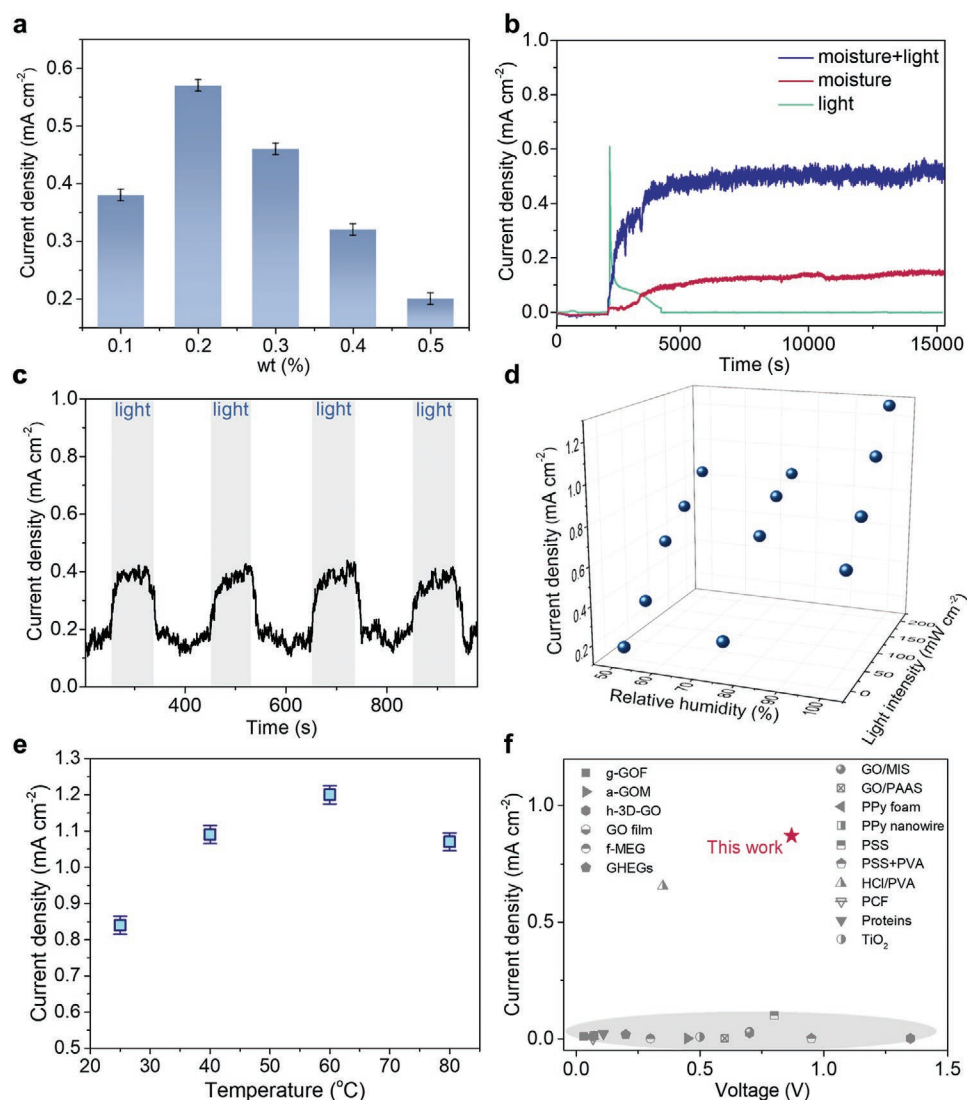
Figure 2. Electric generation of an LMEG unit. a) The dependence of I_{sc} on different content (wt%) of R in PSSA/R film under 50% RH, 100 mW cm^{-2} illumination. b) I_{sc} of LMEG in response to moisture and light, respectively. c) Transient response of LMEG to chopped light under sustained 50% RH (bias = 0 V). d) I_{sc} of LMEG under different RH (50–100%) and light intensity (0–200 mW cm^{-2}) at 25 °C. e) The peak value of I_{sc} as a function of ambient temperature under 50% RH and 200 mW cm^{-2} illumination. f) A systematic performance comparison of the reported MEGs based on various macroscopic devices with inert electrodes (Table S4, Supporting Information).[7,8,10,13]

2.2. Mechanism Verification

The mechanism of sunlight-coordinated moist-electric generation could be proposed as follows. When moisture approaches to the film through the porous upper electrode, the sulfonate groups in PSSA will spontaneously dissociate and release moveable H$^+$ ions.[8c] The different hydration level between upper and bottom side of film leads to gradient distribution of H$^+$ ions across PSSA/R film, which will drive free H$^+$ ions directionally to move with water penetration deeply into the film (**Figure 3**a). In contrast, the negatively charged —SO$_3^-$ groups anchored onto polymer skeletons are immobile. As a result, substantial confinement of —SO$_3^-$ and transport of H$^+$ ions achieve negative/positive charge separation to induce an electric field. Once water adsorption in LMEG approaches saturation, the electricity generation

will decay to zero (Figure S6, Supporting Information).[8c,9,13c] The reversible electricity generation of LMEG can be achieved by water dehydration and subsequent water adsorption repeatedly.

On the other hand, PSSA/R can harvest photons to inspire nonequilibrium carriers upon illumination. When light incidents after moisture incoming, the electric field induced by moisture will facilitate the photogenerated e$^-$ transfer for supplementing negative charge (Figure 3b; Figure S24, Supporting Information).[19] Simultaneously, the migration and redistribution of H$^+$ ions in PSSA during moisture permeability can affect the energy barrier of e$^-$/h$^+$ recombination in R, thus improving e$^-$/h$^+$ separation efficiently for carrier supplement in LMEG.[20] Besides, the introduced PEDOT:PSS layer sandwiched between PSSA/R film and the bottom electrode will act as h$^+$-transport assisting layer, which reduces possibility of e$^-$ moving to the

**ADVANCED
SCIENCE NEWS**

www.advancedsciencenews.com

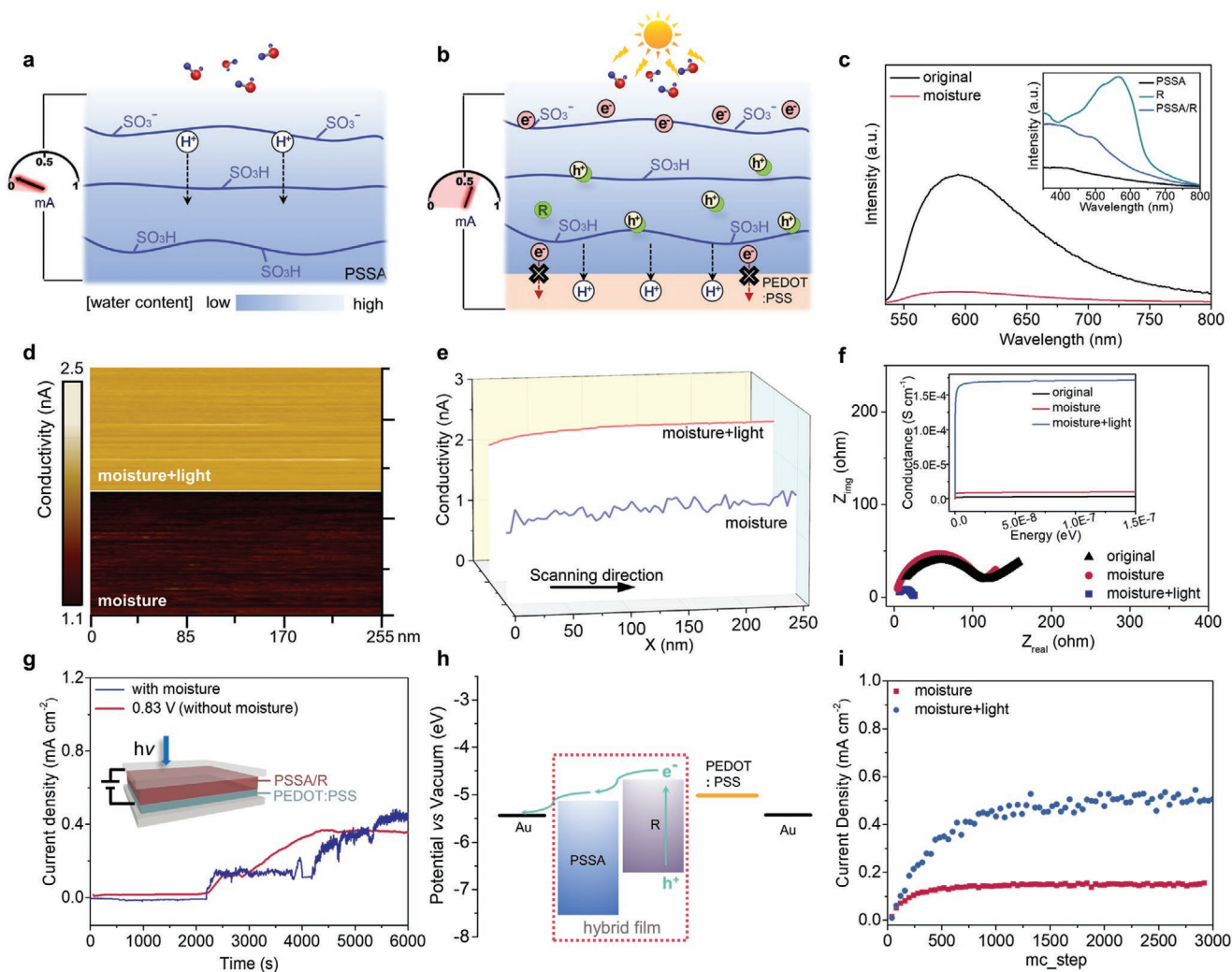**ADVANCED
MATERIALS**

www.advmat.de

Figure 3. Proposed mechanism of an LMEG. a) The functional groups in PSSA are ionized by incoming moisture and releases H^{+} ions. These free H^{+} ions move to the other side leaving negatively charged —SO₃^{−} groups. The positive/negative charge separation induces an electric field. b) R in PSSA matrix are excited by illumination. Photogenerated carriers efficiently migrate under moisture-induced electric field, further enhancing I_{sc} output. Hole (h[+])-transport assisting layer of PEDOT:PSS impedes electron (e[−]) transit, strengthening directional migration of carriers. c) Photoluminescence (PL) spectra of original PSSA/R film and the film standing in 50% RH. Inset: UV–vis absorption curves of PSSA, R and PSSA/R film. d) CAFM images of the surface in PSSA/R film show current mapping. e) The corresponding current distribution of PSSA/R film under moisture (50% RH) and illumination (100 mW cm^{−2}), respectively. The PSSA/R film is rubbed by an Ir-based tip with Pt coating in contact mode. This measured current flows through PSSA/R film between AFM tip and carbon substrate. f) The electrochemical impedance of PSSA/R film in response to moisture (RH = 50%) and light (100 mW cm^{−2}), respectively. The inset shows the dependence of conductance in PSSA/R film on moisture (RH = 50%) and light (100 mW cm^{−2}), separately. g) The comparable I_{sc} of LMEG in response to humidity (50% RH) and extra applied bias (0.83 V) under 100 mW cm^{−2} illumination. Insert: scheme of an LMEG applied with extra bias. h) The electronic band structure diagrams of PSSA, R, PEDOT:PSS, and Au. i) Simulation of current density as a function of mc_steps for moisture only and moisture accompanied with light (parameters see Tables S6 and S7, Supporting Information).

bottom electrode.[21] The existence of PEDOT:PSS layer could further tailor inner carrier migration direction that would synergize well with the direction of H^{+} ions diffusion in LMEG. As a result, light coordination is speculated to largely enrich the available carriers participating in moisture-enabled electric generation, and the electric field induced by moisture could synchronously prompt photogenerated carrier migration, thus boosting electric output in the external circuit synergistically.[22]

The rational introduction of R components extends the absorption spectra of PSSA to 600 nm and enhances the absorption capacity for efficient light harvesting in hybrid film

(inset of Figure 3c). The light absorption of R and photocurrent of the LMEG show the similar dependence on wavelengths (Figure S25, Supporting Information). It demonstrates that photoexcited carriers are proportional to the absorptivity difference of phytochrome.[14a] The efficient e[−]/h[+] separation is verified by the strong photoluminescence quenching of PSSA/R film at RH = 50%. The PL intensity of the same film without moisture adsorption is almost 11 times that of PSSA/R film at RH = 50% (Figure 3c). Furthermore, this reduced PL peak will not appear in pure PSSA or R film after moisture adsorption (Figure S26, Supporting Information), which suggests

that electric field induced by moisture could substantially suppress the unfavorable charge recombination in PSSA/R film. Certainly, permittivity of PSSA and PSSA/R film indicate that this composite construction significantly contributes to e^-/h^+ generation and migration process for carrier supplement (Figure S27a,b, Supporting Information).

In addition, conductive-probe atom force microscopy (CAFM) presents 2D mapping of the current distribution indicating the conductivity of PSSA/R film (Figure 3d). The measured conductivity of hybrid film in 50% RH will increase as exposed to 100 mW cm^{-2} illumination (Figure 3e).[23] Furthermore, in contrast to that of original PSSA/R film, the smaller semicircle in the Nyquist plot of the sample exposed to moisture and illumination (Figure 3f; Figure S27c, Supporting Information) means the enhanced ionic conductivity owing to photogenerated carries.[20] The concrete value in conductivity is determined by

$$\sigma = \frac{L}{R \times S} \tag{2}$$

where σ is the ionic conductivity, L is the thickness, S is the electrode area, and $R = Z_{real}/|Z|$.[24] The original PSSA/R film is 3.1 µS cm^{-1}, which increases to 170 µS cm^{-1} upon moisture and illumination (inset of Figure 3f). The decrease in resistance appears in the results of four-point square resistance measurements (Figure S27d, Supporting Information). The original sheet resistance of 1.2×10^5 Ω $\square^{-1}$ declined to 1.3×10^4 Ω $\square^{-1}$ under 50% RH, whereafter it plunged to 100 Ω $\square^{-1}$ once light on. These above evidence reveals that the enhanced power output of LMEG could be attributed to the increase of carriers in PSSA/R under moisture and light, which is consistent with experimental results in Figure 1e.

For comparison, when water adsorption process is blocked, it fails to induce the potential difference between two sides of a PSSA/R film. Light illumination causes the swift but transient enhancement in electric generation due to the lack of effective photogenerated carrier migration. The e^-/h^+ would generate and recombine with each other rapidly (Figure S28, Supporting Information), whereas, if a preset voltage of the same order of the electric field induced by moisture (i.e., 0.83 V, Figure S6, Supporting Information) was applied between two electrodes (Figure S29, Supporting Information), sustaining current can be detected under irradiation (Figure 3g). Besides, this synergetic effect of moisture and light also depends on rational combination in the composite film. The pure film of PSSA, R, or PEDOT:PSS is incapable to yield comparable electric signal due to the absence of well-matched hybrid construction and tight interaction (Figure S30, Supporting Information). Upon the reception of incident photons, it is energetically favorable for photogenerated e^- in the lowest unoccupied molecular orbital (LUMO) of R transferring to PSSA relying on the band alignment (Figure 3h; Figure S31, Supporting Information). The electric field induced by moisture could strengthen this charge carrier migration. The affected barrier height due to PEDOT:PSS would further tailor the direction of carrier migration. It is confirmed by control experiments. When h$^+$-assisting layer sandwiched between the upper electrode and PSSA/R film, e^- will be impeded to approach the upper electrode so that illumination fail to enhance I_{sc} (Figure S32, Supporting Infor-

mation). In consequence, the electricity generation of LMEG is associated well with spontaneous water adsorption, ions diffusion and photocarrier migration in PSSA/R film. Given different hydration level between two sides of PSSA/R film under moisture, directional transport of H$^+$ ions will spontaneously realize charge separation and induce an electric output. This electric field would promote photoexcited e^-/h^+ to migrate for carrier supplement when light incidents to LMEG. The abundant movable charge carriers accordingly enhance power generation, which can be supported by the dynamical Monte Carlo model coupled with the first reaction method.[25] The calculated I_{sc} will enhance after water adsorption and light illumination (Figure 3i; Figures S33 and S34, Note S1, Supporting Information), in according with the experimental results. It further indicates the rationality of the above proposed mechanism. In addition, the variation in chemical potential energy from gaseous water in air to the adsorbed water in the device and solar energy are the input energy source in this process of electricity generation in LMEG. The energy conversion efficiency is estimated to be about 0.1% (Note S2, Supporting Information).

To verify the above model once again, we further combine other polyelectrolytes with available phytochrome to form different composite films and assemble them into devices with various electrodes (Figures S35–S39, Supporting Information). These polyelectrolytes with structural features similar to PSSA can release free H$^+$ ions and fasten negatively charged immobile polymer chains under moisture (Figure S36, Supporting Information). Composite films such as poly(acrylic acid)/R, hydroxyethyl cellulose/R, poly(vinyl alcohol)/R are tested in the same experimental setup as that for PSSA/R. As expected, they have yielded favorable electric output of 0.1 µA cm^{-2} to 0.1 mA cm^{-2} under moisture and light (Figure S37a, Supporting Information). In addition, the hybrid film comprised with PSSA and other phytochrome also exhibits analogous electric output (Figure S37b, Supporting Information) although different hydrophilic capacity of polyelectrolytes, absorption coefficient of phytochromes, and coupling effect between them result in variable electric generation abilities. These results indicate the mechanism universality of this LMEG model.

2.3. Scalable Integration of LMEGs

The scalable integration of electric generators is critical for realizing highly efficient power output in ambient environment. Notably, the area of one LMEG unit varies ranging from 0.25 to 25 cm^2 (Figure S40, Supporting Information). The output voltage could be enhanced by proper connection. For example, 5.5 V voltage could be easily reached by connecting six LMEG units of 0.25 cm^2 in series (**Figure 4**a). By enlarging the device area, a 25 cm^2 unit can achieve stable current of 1.67 mA and voltage of 0.82 V (Figure 4b,c). It realizes the record-high area and current of single MEG unit with inert electrodes and overcomes the obstacles in low current of electricity generators induced by moisture only (Table S5, Supporting Information). This power output is sufficient to directly run many common electronic devices free of capacitors or rectifiers as shown in Figure S41 and Video S1, Supporting Information. An integrated system with the size of 125 cm^2 offers high voltage and
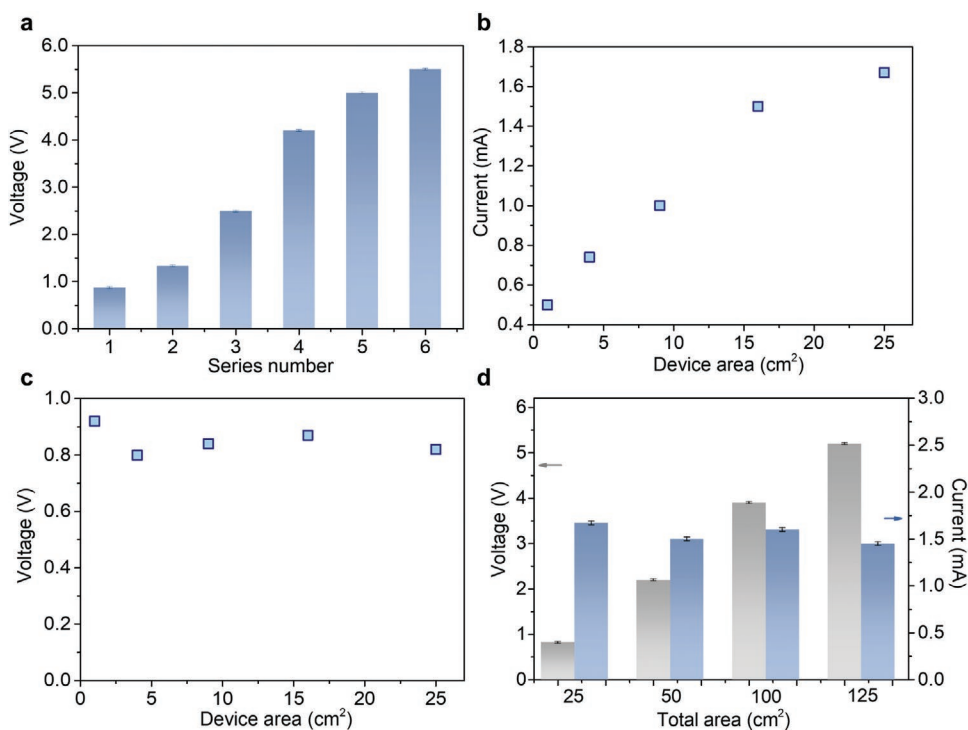
Figure 4. Performance of Integrated LMEGs. a) The V_{oc} output of 0.25 cm² LMEG units connected in series. b) I_{sc} and c) V_{oc} output of one LMEG unit with different area. d) V_{oc} and I_{sc} output of assembled LMEG packages in which 1–5 LMEG units of 25 cm² are connected in series, respectively. The testing conditions are 50% RH, and 100 mW cm⁻² illumination.

current synchronously (Figure 4d), confirming the scaling performance of LMEGs. Therefore, these considerable and steady power output make them practicable to integrate LMEGs for scalable applications under different natural environment.

To meet the flexible and scalable applications, the LMEGs are integrated on arbitrary substrates, such as poly(ethylene terephthalate) (PET) films, glasses, papers, metals, and clothes. Due to pliant nature of PSSA/R film, flexible LMEGs (f-LMEGs) can be fabricated conveniently. The f-LMEGs will be suitable for portable objects to harvest energy from various natural conditions without temporal and geographical limitation.

During October 2020, we tested the power generation performance of integrated LMEGs on the campus of Tsinghua University, Beijing. For example, flexible f-LMEGs can be bent arbitrarily and connected in series to wrap around a cup, which provide enough power to run a commercial temperature–humidity monitor (**Figure 5**a). In addition, the electricity power supplied by LMEGs can be stored into commercial energy-storage devices without extra rectifiers (Figure 5b). Specially, adequate moist air and sunlight near a lake provide an appropriate scene for f-LMEGs working on a boat to charge a capacitor up to 5.5 V voltage and 1 F capacitance within about 9h (Figure S42, Supporting Information). It is sufficient to drive blade rotation, thus sailing a small speedboat on water (Figure 5c; Video S2, Supporting Information). The wearable system is composed of LMEGs designed with a commercial cloth. Even at relatively low RH of 30% and light intensity of 30 mW cm⁻², this wearable system can harvest ambient moisture and sunlight spontaneously charging for a capacitor during the day. Subsequently, a flashlight is lit up, relying on energy stored in the capacitor

at night (Figure 5d). It is convenient for outdoor travel or long-time operation especially. This scalable integrated system based on LMEGs could be installed on various buildings. As shown in Figure 5e, large-scale LMEGs are constructed onto the roof of a house model to serve as power supply system. It is capable of powering lighting and electrically driven objects directly upon exposure to the natural environment without any other auxiliaries (Video S3, Supporting Information). These practical applications demonstrate the great potential of LMEGs for powering household and outdoor electrical appliances through environment energy harvesting in the future.

3. Conclusion

A new type of highly efficient sunlight-coordinated moisture power is presented by rational combination of a polyelectrolyte and a phytochrome. A tailorable single piece of PSSA/R film could offer V_{oc} of 0.92 V and I_{sc} of 1.55 mA cm⁻² based on spontaneous adsorption of water molecules and photon harvesting. This synergistic effect contributes to a record-high current density. In the hybrid film, polyelectrolytes will spontaneously cause charge separation and subsequent directional movement of H⁺ ions under moisture, thus inducing an electric output. This electric field tuned by moisture could accordingly drive photogenerated e⁻ migration to significantly enrich carriers in the LMEG under illumination. The synergetic charge carrier transfer further promotes power generation. As expected, this kind of sunlight-coordinated moist-electric generation is also applicable to many other assemblies of polyelectrolytes with

Figure 5. Demonstration of LMEG as practical power source in real life conditions. a) The f-LMEGs bent around a cup could power a temperature–humidity monitor. b) The circuit diagram for applications in (c) and (d). S1: twelve LMEGs in series–parallel connection charging for a capacitor. S2: accumulated energy in the capacitor powering commercial electronics, such as a boat or a flashlight. c) A small speedboat is sailing on the water driven by an LMEG-charged capacitor. d) Left: LMEGs are integrated with garment and charged a capacitor during the day. Right: the electricity stored in the capacitor could light up a flashlight at night. e) LMEGs are installed on the roof of a house model for powering common electronics such as a red LED and an electronic clock in a real natural environment without any other auxiliaries.

phytochromes. Furthermore, LMEG units can be integrated on large scale. Such integration devices produce sufficient power to work for various electronics (e.g., sailing speedboat, flashlight) in wearable and potable system by harvesting energy from ambient environment. The LMEG-based power supply system could be potentially developed for household and outdoor electrical appliances. These findings provide a versatile avenue to develop green and sustainable power generation through comprehensive utilization of natural sources from ambient environment.

4. Experimental Section

Preparation of PSSA/R Film: Rose bengal (R) was mixed with aqueous PSSA solution (M_w = 70 000, 30 wt% in H_2O, Sigma-Aldrich). The mixed solution was cast into a mold and dried over-night in an oven at 37 °C and RH was set as 45%. The hybrid film was obtained with the content (wt%) of R in PSSA/R film of 0.2%. Similarly, poly(acrylic acid)/R, sodium 2-bromoethanesulfonate/R, disodium 3,3′-dithiobis(1-propanesulfonate)/R, hydroxyethyl cellulose/R, PSSA/TMPyP, PSSA/ZnPP, PSSA/RhB, PSSA/FCF, PSSA/Meso-TPP and PSSA/TPPS films could be prepared by the same protocol as PSSA/R film.

Preparation of Pure Film: Pure PSSA solution was cast into a flat bottom mold directly and stood overnight in an oven at 37 °C and 45% RH. Pure R and pure PEDOT:PSS were dissolved into deionized water (30 wt%) and repeated the same steps with pure PSSA film to obtain homogeneous film.

Preparation of Electrodes: Uniformly distributed holes were manufactured on the upper electrode for ventilation and photopermeability. The diameter of the holes was 1.3 mm. A pair of Au electrodes was applied in tests in Figures 1–4 and Figures S1–S43, Supporting Information, except for Figures S23 and S39, Supporting Information. In Figure 5, PET pre-printed with carbon paste and carbon paper served as the electrodes in the flexible LMEG. In Figure S39, Supporting Information, the upper electrodes were FTO glass, stainless-steel panel and mesh covered by Au. The bottom electrodes were carbon paper, Ag, FTO glass covered by Au, PET pre-printed with carbon paste. In Figure S23, Supporting Information, Al was utilized in the electrodes of the LMEG. Al electrodes will not be used in other measurements.

Fabrication of LMEG: PEDOT:PSS solution was spin-coated on the bottom electrode. The electrode was dried in an oven at 50 °C. Immediately, a formed composite film was sandwiched between two electrodes and inserted into a test circuit in an enclosed container with an RH controlling system for electrical measurements.

Electric Measurement: All the voltage and current signals were recorded by a Keithley 2400 multimeter, which was controlled by a LabView-based data acquisition system. The circuit parameters of the V_{oc} test were current = 0 mA and step index = 10 points s^{-1}. The circuit parameters of the I_{sc} test were voltage = 0 V and step index = 10 points s^{-1}. A 300 W Xe lamp (Beijing MerryChange Technology Co. Ltd.) with the intensity of 100 mW cm^{-2} was utilized as the light source. The temperature distribution of devices were recorded by an IR camera (Fluke).

Material Characterization: The morphology and microstructures of films were characterized using a scanning electron microscope (FLexSEM 1000) and a confocal laser scanning microscope (FV 10i-O,

Olympus). Fourier transform infrared spectroscopy (FTIR) testing was conducted on Nicolet 6700FTIR. X-ray photoelectron spectroscopy (XPS) spectra were recorded with photoelectron spectrometer (PHI Quantera II Ulvac-Phi Incorporation) with Al Kα. Ultraviolet photoelectron spectrometry (UPS, ESCALab250Xi) was performed to determine the valence band edges of PSSA and R. The UV–vis absorption spectra were recorded on a DR/5000 spectrophotometer. PL spectra were carried out in an Edinburgh FLSP920 fluorimeter. The conductive atomic force microscopy experiments were conducted using a scanning probe microscopy system (DIMENSION ICON, BRUKER) at CAFM mode. Electrochemical impedance spectroscopy (EIS), conductivity, and permittivity were obtained from broadband dielectric impedance spectrometer (CONCEPT-80, NOVOCONTROT). Sheet resistance was detected by four-probe thin layer resistance tester (280SJ, 4 Dimensions). Differential scanning calorimetry (DSC, Q5000IR) was used to measure the specific heat capacity of the samples. The mass change of the samples under different temperature and different RH was tested by dynamic vapor sorption (DVS Adventure).

Device Physics Model: Dynamical Monte Carlo simulation with first reaction algorithm on a lattice of $50 \times 50 \times 100$ was employed to simulate the current and voltage generated by moisture diffusion as well as illumination, in analogy to our previous work on organic photovoltaic device simulations.[25] At each site, events could occur: proton generation, proton hopping, exciton generation, exciton dissociation, electron and hole hopping, and charge collection at the boundaries. The flowchart and the parameters employed in the simulation can be found in Note S1, Supporting Information.

Supporting Information

Supporting Information is available from the Wiley Online Library or from the author.

Acknowledgements

Conflict of Interest

The authors declare no conflict of interest.

Data Availability Statement

Research data are not shared.

Keywords

[1] F. Bonaccorso, L. Colombo, G. Yu, M. Stoller, V. Tozzini, A. C. Ferrari, R. S. Ruoff, V. Pellegrini, *Science* **2015**, *347*, 1246501.

[2] W. Li, L. Ye, S. Li, H. Yao, H. Ade, J. Hou, *Adv. Mater.* **2018**, *30*, 1707170.

[3] F. P. García Márquez, A. M. Tobias, J. M. Pinar Pérez, M. Papaelias, *Renewable Energy* **2012**, *46*, 169.

[4] S. Lin, W. Li, Z. Chen, J. Shen, B. Ge, Y. Pei, *Nat. Commun.* **2016**, *7*, 10287.

[5] a) Y. Zi, J. Wang, S. Wang, S. Li, Z. Wen, H. Guo, Z. L. Wang, *Nat. Commun.* **2016**, *7*, 10987; b) Z. L. Wang, J. Song, *Science* **2006**, *312*, 242.

[6] a) H. Cheng, J. Liu, Y. Zhao, C. Hu, Z. Zhang, N. Chen, L. Jiang, L. Qu, *Angew. Chem., Int. Ed.* **2013**, *52*, 10482; b) Z. Zhang, X. Li, J. Yin, Y. Xu, W. Fei, M. Xue, Q. Wang, J. Zhou, W. Guo, *Nat. Nanotechnol.* **2018**, *13*, 1109; c) J. Bai, Y. Huang, H. Cheng, L. Qu, *Nanoscale* **2019**, *11*, 23083; d) T. Xu, H. Qing, Z. Cheng, J. Zhang, L. Qu, *Small Methods* **2018**, *2*, 1800108; e) Y. Han, Z. Zhang, L. Qu, *FlatChem* **2019**, *14*, 100090; f) Y. Xu, P. Chen, H. Peng, *Chem. - Eur. J.* **2018**, *24*, 6287. g) Y. Zhang, D. K. Nandakumar, S. C. Tan, *Joule* **2020**, *4*, 2532; h) X. Zhang, J. Yang, R. Borayek, H. Qu, D. K. Nandakumar, Q. Zhang, J. Ding, S. C. Tan, *Nano Energy* **2020**, *75*, 104873; i) J. Yang, X. Zhang, H. Qu, Z. G. Yu, Y. Zhang, T. J. Eey, Y. W. Zhang, S. C. Tan, *Adv. Mater.* **2020**, *32*, 2002936.

[7] a) F. Zhao, H. Cheng, Z. Zhang, L. Jiang, L. Qu, *Adv. Mater.* **2015**, *27*, 4351; b) F. Zhao, Y. Liang, H. Cheng, L. Jiang, L. Qu, *Energy Environ. Sci.* **2016**, *9*, 912; c) Y. Huang, H. Cheng, C. Yang, P. Zhang, Q. Liao, H. Yao, G. Shi, L. Qu, *Nat. Commun.* **2018**, *9*, 4166; d) H. Cheng, Y. Huang, F. Zhao, C. Yang, P. Zhang, L. Jiang, G. Shi, L. Qu, *Energy Environ. Sci.* **2018**, *11*, 2839.

[8] a) T. Xu, X. Ding, C. Shao, L. Song, T. Lin, X. Gao, J. Xue, Z. Zhang, L. Qu, *Small* **2018**, *14*, 1704473; b) Y. Liang, F. Zhao, Z. Cheng, Y. Deng, Y. Xiao, H. Cheng, P. Zhang, Y. Huang, H. Shao, L. Qu, *Energy Environ. Sci.* **2018**, *11*, 1730; c) T. Xu, X. Ding, Y. Huang, C. Shao, L. Song, X. Gao, Z. Zhang, L. Qu, *Energy Environ. Sci.* **2019**, *12*, 972; d) Y. Huang, H. Cheng, C. Yang, H. Yao, C. Li, L. Qu, *Energy Environ. Sci.* **2019**, *12*, 1848; e) H. Wang, H. Cheng, Y. Huang, C. Yang, D. Wang, C. Li, L. Qu, *Nano Energy* **2020**, *67*, 104238.

[9] A. T. Liu, Y. Kunai, A. L. Cottrill, A. Kaplan, G. Zhang, H. Kim, R. S. Mollah, Y. L. Eatmon, M. S. Strano, *Nat. Commun.* **2021**, *12*, 3415.

[10] H. Wang, Y. Sun, T. He, Y. Huang, H. Cheng, C. Li, D. Xie, P. Yang, Y. Zhang, L. Qu, *Nat. Nanotechnol.* **2021**, *16*, 811.

[11] a) J. Q. Wu, R. D. Zhang, S. X. Gui, *Plant Soil* **1999**, *215*, 7; b) C. X. Zhao, X. P. Deng, S. Q. Zhang, Q. Ye, E. Steudle, L. Shan, *J. Integr. Plant Biol.* **2004**, *46*, 505; c) W. Yamori, K. Hikosaka, D. A. Way, *Photosynth. Res.* **2014**, *119*, 101; d) S. L. Nielsen, *Aquat. Bot.* **1993**, *45*, 27.

[12] a) H. Van, P. Lee, N. R. Armstrong, A. Graham, G. A. Evmenenko, P. Dutta, T. J. Marks, *J. Am. Chem. Soc.* **2005**, *127*, 3172; b) S. Y. Shao, J. Liu, J. Bergqvist, S. W. Shi, C. Veit, U. Wurfel, Z. Y. Xie, F. L. Zhang, *Adv. Energy Mater.* **2013**, *3*, 349.

[13] a) Y. Liang, F. Zhao, Z. H. Cheng, Q. H. Zhou, H. B. Shao, L. Jiang, L. T. Qu, *Nano Energy* **2017**, *32*, 329; b) F. Zhao, L. X. Wang, Y. Zhao, L. T. Qu, L. M. Dai, *Adv. Mater.* **2016**, *29*, 1604972; c) Y. X. Huang, H. H. Cheng, G. Q. Shi, L. T. Qu, *ACS Appl. Mater. Interfaces* **2017**, *9*, 38170; d) H. H. Cheng, Y. X. Huang, L. T. Qu, Q. L. Cheng, G. Q. Shi, J. Lan, *Nano Energy* **2017**, *45*, 37; e) C. X. Shao, J. Gao, T. Xu, B. X. Ji, Y. K. Xiao, C. Gao, Y. Zhao, L. T. Qu, *Nano Energy* **2018**, *53*, 698; f) C. Yang, Y. X. Huang, H. H. Cheng, L. Jiang, L. T. Qu, *Adv. Mater.* **2019**, *31*, 1805705; g) K. Liu, P. H. Yang, S. Li, J. Li, T. P. Ding, G. B. Xue, Q. Chen, G. Feng, J. Zhou, *Angew. Chem., Int. Ed.* **2016**, *55*, 8003; h) M. J. Li, L. Zong, W. Q. Yang, X. K. Li, J. You, X. C. Wu, Z. H. Li, C. X. Li, *Adv. Funct. Mater.* **2019**, *29*, 1901798; i) J. L. Xue, F. Zhao, C. G. Hu, Y. Zhao, H. X. Luo, L. M. Dai, L. T. Qu, *Adv. Funct. Mater.* **2016**, *26*, 8784; j) X. W. Nie,

**ADVANCED
SCIENCE NEWS**

www.advancedsciencenews.com

**ADVANCED
MATERIALS**

www.advmat.de

B. X. Ji, N. Chen, Y. Liang, Q. Han, L. T. Qu, *Nano Energy* **2018**, *46*, 297; k) Z. L. Luo, C. H. Liu, S. S. Fan, *Nano Energy* **2019**, *60*, 371; l) D. Z. Shen, M. Xiao, G. S. Zou, L. Liu, W. W. Duley, Y. N. Zhou, *Adv. Mater.* **2018**, *30*, 1705925.

[14] R. B. Adler, A. C. Smith, R. L. Longini, *Introduction to Semiconductor Physics, Semiconductor Electronics Education Committee Books*, Vol. *1*, John Wiley & Sons, Inc., New York **1964**, p. 79.

[15] a) J. Bai, B. Lu, Q. Han, Q. Li, L. Qu, *ACS Appl. Mater. Interfaces* **2018**, *10*, 38066; b) D. Mateo, I. Esteve-Adell, J. Albero, J. Royo, A. Primo, H. Garcia, *Nat. Commun.* **2016**, *7*, 11819.

[16] Z. H. Wu, Y. C. Zhai, W. C. Yao, N. Eedugurala, S. Zhang, L. F. Huang, X. D. Gu, J. D. Azoulay, T. Ng, *Adv. Funct. Mater.* **2018**, *28*, 1805738.

[17] L. B. Luo, D. Wang, C. Xie, J. Hu, X. Y. Zhao, F. X. Liang, *Adv. Funct. Mater.* **2019**, *29*, 1900849.

[18] Y. Q. Zhan, J. Qin, A. A. Umar, J. Wang, X. Zhang, H. Wang, X. Cui, X. Li, L. Zheng, Y. Zhan, *Adv. Funct. Mater.* **2019**, *29*, 1902234.

[19] a) Q. S. Lv, F. G. Yan, X. Wei, K. Y. Wang, *Adv. Opt. Mater.* **2017**, *6*, 1700490; b) N. Ma, Y. Yang, *Nano Energy* **2019**, *60*, 95.

[20] J. Maier, D. Moia, A. Senocrate, G. Y. Kim, Y. Wang, *Angew. Chem., Int. Ed.* **2021**, *133*, 833.

[21] L. X. Zheng, X. L. Deng, Y. Z. Wang, J. X. Chen, X. S. Fang, L. Wang, X. W. Shi, H. J. Zheng, *Adv. Funct. Mater.* **2020**, *30*, 2001604.

[22] F. Gallego-Gómez, E. M. García-Frutos, J. M. Villalvilla, J. A. Quintana, E. Gutierrez-Puebla, A. Monge, A. M. Díaz-García, B. Gómez-Lor, *Adv. Funct. Mater.* **2011**, *21*, 738.

[23] L. Su, H. Y. Li, Y. Wang, S. Y. Kuang, Z. L. Wang, G. Zhu, *Nano Energy* **2016**, *31*, 264.

[24] C. Han, X. Qian, Q. Li, B. Deng, Y. Zhu, Z. Han, W. Zhang, W. Wang, S. Feng, G. Chen, W. Liu, *Science* **2020**, *368*, 1091.

[25] a) R. A. Marsh, C. Groves, N. C. Greenham, *J. Appl. Phys.* **2007**, *101*, 083509; b) P. K. Watkins, A. B. Walker, G. L. B. Verschoor, *Nano Lett.* **2005**, *5*, 1814; c) L. Y. Meng, Y. Shang, Q. K Li, Y. F. Li, X. W. Zhan, Z. G. Shuai, R. G. E. Kimber, A. B. Walker, *J. Phys. Chem. B* **2010**, *114*, 36.